# Lower Order Harmonics Reduction In A Grid Connected Single Phase PV Inverter

**U. V. Eswarudu[1], T. Lakshminarayana[2], G. Kirankumar[3]**
[1, 2, 3] Department of Electrical and Electronics Engineering
[1, 2, 3] Kakinada Institute of Technology and Science

***Abstract-*** *In this paper, a simple single-phase grid-connected photovoltaic (PV) inverter topology consisting of a boost section, a low-voltage single-phase inverter with an inductive filter, and a step-up transformer interfacing the grid is considered. Ideally, this topology will not inject any lower order harmonics into the grid due to high-frequency pulse width modulation operation.*

*However, the non ideal factors in the system such as core saturation-induced distorted magnetizing current of the transformer and the dead time of the inverter, etc., contribute to a significant amount of lower order harmonics in the grid current. A novel design of inverter current control that mitigates lower order harmonics is presented in this paper. An adaptive harmonic compensation technique and its design are proposed for the lower order harmonic compensation.*

*In addition, a proportional-resonant-integral (PRI) controller and its design are also proposed. This controller eliminates the dc component in the control system, which introduces even harmonics in the grid current in the topology considered. The performance of the system due to the interaction between the PRI controller and the adaptive compensation scheme is also analyzed. The complete design has been validated with experimental results and good agreement with theoretical analysis of the overall system is observed.*

***Keywords-*** Adaptive filters, harmonic distortion, inverters, solar energy.

## I. INTRODUCTION

Renewable sources of energy such as solar, wind, and geothermal have gained popularity due to the depletion of conventional energy sources. Hence, many distributed generation (DG) systems making use of the renewable energy sources are being designed and connected to a grid. In this paper, one such DG system with solar energy as the source is considered. The topology of the solar inverter system is simple. It consists of the following three power circuit stages:

1) A boost converter stage to perform maximum power point tracking (MPPT);
2) A low-voltage single-phase *H*-bridge inverter;
3) An inductive filter and a step-up transformer for interfacing with the grid.

Fig. 1 shows the power circuit topology considered. This topology has been chosen due to the following advantages: The switches are all rated for low voltage which reduces the cost and lesser component count in the system improves the overall reliability. This topology will be a good choice for low-rated PV inverters of rating less than a kilowatt. The disadvantage would be the relatively larger size of the interface transformer compared to topologies with a high-frequency link transformer [1].

The system shown in Fig.1will not have any lower order harmonics in the ideal case. However, the following factors result in lower order harmonics in the system: The distorted magnetizing current drawn by the transformer due to the nonlinearity in the *B–H* curve of the transformer core, the dead time introduced between switching of devices of the same leg [2]–[6], on-state voltage drops on the switches, and the distortion in the grid voltage itself.

There can be a dc injection into the transformer primary due to a number of factors. These can be the varying power reference from a fast MPPT block from which the ac current reference is generated, the offsets in the sensors, and A/D conversion block in the digital controller. This dc injection would result in even harmonics being drawn from the grid, again contributing to a lower power quality.

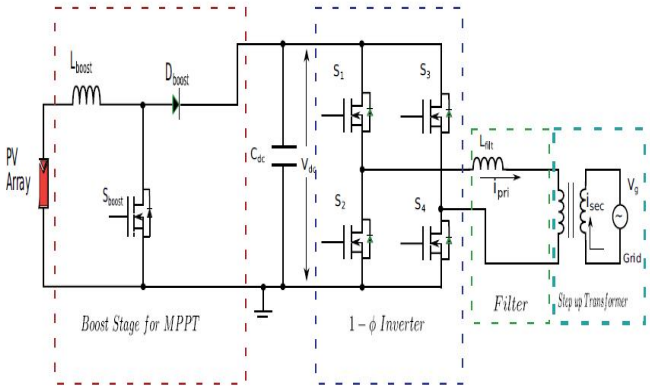


Figure 1 Power circuit topology of a single phase low voltage PV inverter

It is important to attenuate these harmonics in order for the PV inverter to meet standards such as IEEE 519-1992 [7] and IEEE 1547-2003 [8]. Hence, this project concentrates on the design of the inverter current control to achieve a good attenuation of the lower order harmonics. It must be noted that attenuating the lower order harmonics using a larger output filter inductance is not a good option as it increases losses in the system along with a larger fundamental voltage drop and with a higher cost. The boost stage and the MPPT scheme are not discussed in this paper as a number of methods are available in the literature to achieve a very good MPPT [9]–[13].

There has been considerable research work done in the area of harmonic elimination using specialized control. In [15]–[22], multi resonant controller-based methods are used for selective harmonic elimination. The advantage of these methods is the simplicity in implementation of the resonant blocks. However, discretization and variations in grid frequency affect the performance of these controllers and making them frequency adaptive increases overall complexity [21], [22]. Also, as mentioned in [19], [21], and [22], the phase margin of the system becomes small with multi resonant controllers and additional compensation is required for acceptable operation. The study in [23]–[25] considers the use of repetitive controller-based harmonic elimination which involves complicated analysis and design. As mentioned in [26], the performance of the repetitive controller is very sensitive to frequency variations and needs structural change for better performance, which might affect the stability.

In [27]–[31], adaptive filter-based controllers are considered for harmonic compensation. The study in [27] uses an adaptive filter to estimate a harmonic and then adds it to the main current reference. Then, a multiresonant block is used to ensure zero steady-state error for that particular harmonic reference. Thus, the study in [27] uses both adaptive and multi resonant schemes increasing overall complexity. Similar approaches are found in [28] and [29] which add the harmonic current reference estimated using adaptive filters and use a hysteresis controller for the reference tracking. Usage of a hysteresis controller makes it difficult to quantify the effectiveness of this scheme. The study in [30] uses an adaptive filter-based method for dead-time compensation in rotating reference frame, which is not suitable in single-phase systems. The method proposed in [31] requires an inverse transfer function of the system and is proposed for grid-connected topology assuming the connection to be purely inductive.

## II. LOWER ORDER HARMONICS AND FUNDAMENTAL CURRENT CONTROL

This section discusses the origin of the lower order harmonics in the system under consideration. The sources of these harmonics are not modeled as the method proposed to attenuate those works independent of the harmonic source. The fundamental current control using the proposed PRI controller is also explained.

### A) Origin of Lower Order Harmonics

#### a) Odd Harmonics

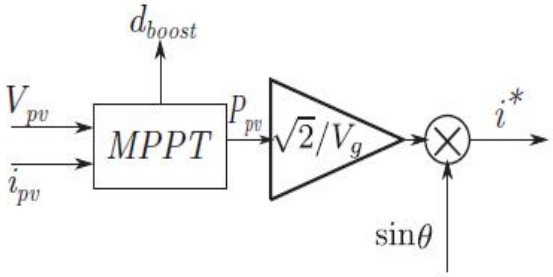


Figure 2 Generation of an inverter ac current reference from an MPPT block

The magnetizing current lags the grid voltage by 90◦. Hence, the harmonic currents will have a phase displacement of either +90◦ or −90◦ depending on harmonic order. The dead-time effect introduces lower order harmonics which are proportional to the dead time, switching frequency, and the dc bus voltage. The dead-time effect for each leg of the inverter can be modeled as a square wave error voltage out of phase with the current at the pole of the leg [2]–[6]. The device drops also will cause a similar effect but the resulting amount of distortion is smaller compared to that due to the dead time. Thus, for a single-phase inverter topology considered, net error voltage is the voltage between the poles and is out of phase with the primary current of the transformer. The harmonic voltage amplitude for a *h*th harmonic can be expressed as

$$V_{\text{error}} = \frac{4}{h\pi}\frac{2V_{\text{dc}}t_d}{T_s}$$

where $t_d$ is the dead time, *Ts* is the device switching frequency, and $V_{\text{dc}}$ is the dc bus voltage. Using the values of the filter inductance, transformer leakage inductance, and the net series resistance, the harmonic current magnitudes can be evaluated. Again, it must be noted that the phase angle of the harmonic currents in this case will be 180◦ for UPF operation. Thus, it can be observed that the net harmonic content will have some phase angle with respect to the fundamental current depending

on the relative magnitudes of the distortions due to the magnetizing current and the dead time.

**b) Even Harmonics**

The topology under consideration is very sensitive to the presence of dc offset in the inverter terminal voltage. The dc offset can enter from a number of factors such as varying power reference given by a fast MPPT block, the offsets in the A/D converter, and the sensors. To understand how a fast MPPT introduces a dc offset, consider Figs.2 and 3. In boost is the duty ratio command given to the boost converter switch, *V*pv and *i*pv are the panel voltage and current, respectively, *P*pv is the panel output power, *Vg* is the rms value of the grid voltage, sin $\theta$ is the in-phase unit vector for the grid voltage, and $i^*$ is the reference to the current control loop from an MPPT block. As the power reference keeps on changing due to fast MPPT action, the current reference may have a nonzero average value, which is illustrated in Fig. 3 for a step change in power reference which repeats.

Assume that a certain amount of dc exists in the current control loop. This will result in applying a voltage with a dc offset across the *L*-filter and the transformer primary. The net average current flowing in the filter and the transformer primary loop will be determined by the net resistance present in the loop. This average current will cause a dc shift in the *B*–*H* curve of the transformer [33]–[35]. This shift would mean an asymmetric nonlinear saturation characteristic which causes the transformer magnetizing current to lose its half-wave symmetry. of this is occurrence of even harmonics.

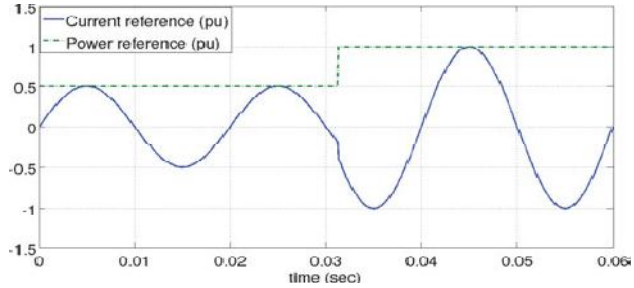


Figure 3 Occurrence of nonzero average in current reference due to a fast changing power reference from MPPT

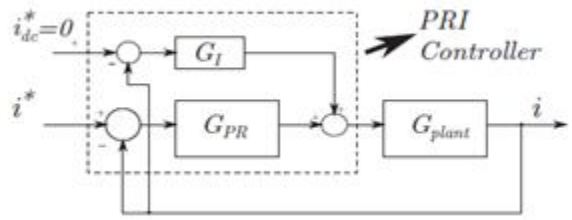


Figure 4 Block diagram of the fundamental current control with the PRI controller

**B) Fundamental Current Control**

**a) Introduction to the PRI Controller**

Conventional stationary reference frame control consists of a PR controller to generate the inverter voltage reference. In this paper, a modification to the PR controller is proposed, by adding an integral block, $G_I$ as indicated in Fig.4.3. The modified control structure is termed as a PRI controller.
Here

$$G_I = \frac{K_I}{s}$$

$$G_{\mathrm{PR}}(s) = K_p + \frac{K_r s}{s^2 + \omega_o^2}.$$

The plant transfer function is modeled as

$$G_{\mathrm{plant}}(s) = \frac{V_{\mathrm{dc}}}{R_s + sL_s}.$$

This is because the inverter will have a gain of *V*dc to the voltage reference generated by the controller and the impedance offered is given by (*Rs* + *sLs* ) in s-domain. *Rs* and *Ls* are the net resistance and inductance referred to the primary side of the transformer, respectively. *Ls* includes the filter inductance and the leakage inductance of the transformer. *Rs* is the net series resistance due to the filter inductor and the transformer.

The PRI controller is proposed to ensure that the output current of the system does not contain any dc offset. The PRI controller introduces a *zero* at *s* = 0in the closed-loop transfer function. Hence, the output current will not contain any steady state dc offset. This is necessary in the topology considered because the presence of a dc offset would result in a flow of even harmonics The following section explains the design of PR controller parameters and proposes a systematic method of selecting and tuning the gain of the integral block in the PRI controller.

## III. ADAPTIVE HARMONIC COMPENSATION

An adaptive filter is a system with a linear filter that has a transfer function controlled by variable parameters and a means to adjust those parameters according to an optimization algorithm. Because of the complexity of the optimization algorithms, most adaptive filters are digital filters.

**A) Adaptive Harmonic Compensation**

In this section, first the LMS adaptive filter is briefly reviewed. Then, the concept of lower order harmonic compensation and the design of the adaptive harmonic compensation block using this adaptive filter are explained. Next, complete current Fig. 6. Step response of closed-loop transfer function $G_{cl}$, PRI for different values of $K_i$ .

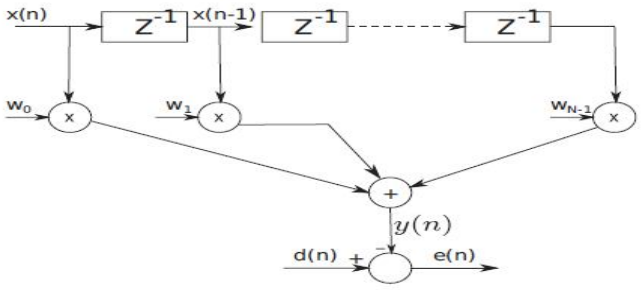


Figure 5 Structure of a generalized adaptive filter with adaptation weights $w_i$

**a) Review of the LMS Adaptive Filter**

The adaptive harmonic compensation technique is based on the usage of an LMS adaptive filter to estimate a particular harmonic in the output current. This is then used to generate a counter voltage reference using a proportional controller to attenuate that particular harmonic. Adaptive filters are commonly used in signal processing applications to remove a particular sinusoidal interference signal of known frequency [37]. Fig.6 shows a general adaptive filter with *N* weights. The weights are adapted by making use of the LMS algorithm.

In any adaptive filter, the weight vector *w* is updated such that the performance function moves toward its minimum. Thus

$$\overline{w}(n+1) = \overline{w}(n) - \mu\nabla(e(n)^2).$$

In (29), $\mu$ is the step size. The convergence of the adaptive filter depends on the step size $\mu$. A smaller value would make the adaptation process very slow whereas a large value can make the system oscillatory. Delta is defined as the gradient of the performance function with respect to the weights of the filter. The final update equation for weights of an LMS adaptive filter can be shown to be [37]

$$w(n+1) = w(n) + 2\mu e(n)x(n).$$

Thus, from a set of known input vector $x(n)$, a signal $y(n)$ is obtained by the linear combination of $x(n)$ and the weight vector $w(n)$ as in (26). Signal $y(n)$ is an estimate of the signal $d(n)$ and the weight vector is continuously updated from (30) such that the LMS error $e(n) = d(n) - y(n)$ is minimized.

This concept can be used to estimate any desired frequency component in a signal $d(n)$. The adaptive filter used for this purpose will take the reference input $x(n)$ as the sine and cosine terms at that desired frequency. The weight vector will contain two components which scale the sine and cosine and add them up to get an estimated signal $y(n)$. The weights will then be adapted in such a way as to minimize the LMS error between $d(n)$ and $y(n)$. In steady state, estimated signal $y(n)$ will equal the frequency component of interest in $d(n)$.

**b) Adaptive Harmonic Compensation**

The LMS adaptive filter discussed previously can be used for selective harmonic compensation of any quantity, say grid current. To reduce a particular lower order harmonic (say $i_k$) of grid current:

1) $i_k$ is estimated from the samples of grid current and phase locked loop (PLL) [38] unit vectors at that frequency;
2) A voltage reference is generated from the estimated value of $i_k$ ;
3) Generated voltage reference is subtracted from the main controller voltage reference.

Fig.6 shows the block diagram of the adaptive filter that estimates the *k*th harmonic $i_k$ of the grid current *i*. The adaptive block takes in two inputs $\sin(k\omega o\ t)$ and $\cos(k\omega o\ t)$ from a PLL.

These samples are multiplied by the weights *W*cos and *W*sin. The output is subtracted from the sensed grid current sample, which is taken as the error for the LMS algorithm. The weights are then updated as per the LMS algorithm and the output of this filter would be an estimate of the *k*th harmonic of grid current. The weights update would be done by using the equations given next, where *Ts* is the sampling time, $e(n)$ is the error of *n*th sample, and $\mu$ is the step size

$$e(n) = i(n) - ik\ (n)$$

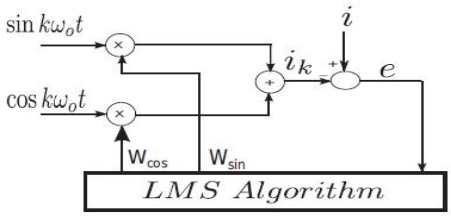


Figure .6 Block diagram of adaptive estimation of a particular harmonic of grid current

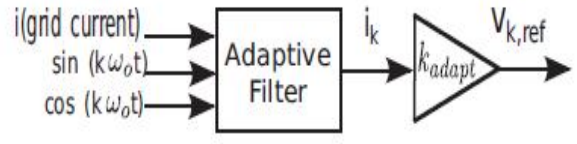


Figure 7 Generation of voltage reference from estimated $k_{th}$ harmonic component of current using the LMS adaptive filter

$$W\cos(n+1) = W\cos(n) + 2\mu e(n)\cos(k\omega onTs)$$
$$W\sin(n+1) = W\sin(n) + 2\mu e(n)\sin(k\omega onTs)$$

**c) Computation of $k_{adapt}$**

Based on the estimated net *k*th harmonic in the grid current, the voltage reference *vk*,ref is generated by multiplying the estimated harmonic with *k*adapt. The effect of this voltage reference is that it results in an amplified voltage at that harmonic frequency at the inverter terminals and this will inject a current at that frequency in the primary side. The reflected secondary current will oppose the original current that was present in the secondary and hence there will be a net reduction in that particular harmonic in the grid current. Consequently, the primary side current will be more distorted. The amount of reduction of the harmonic in grid current will depend on $k_{adapt}$.

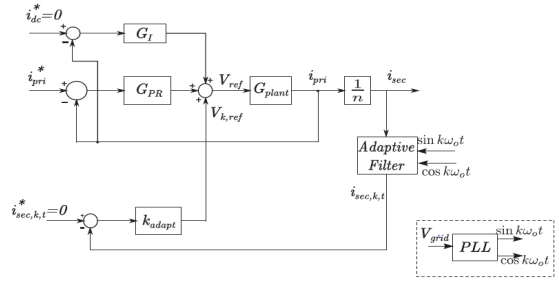


Figure 8 Complete ac current control structure of the inverter

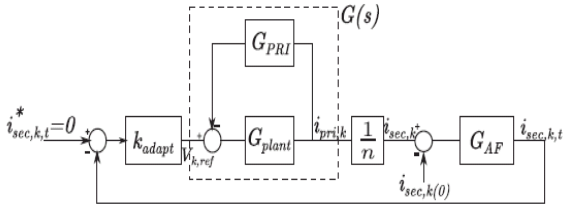


Figure 9 Block diagram for calculating k adapt

To calculate $k_{adapt}$, the control block diagram shown in Fig.9 is used. This block diagram is derived using Fig. 8 by considering the control variable to be regulated as the *k*th harmonic in secondary current. While deriving this harmonic control block diagram, the fundamental reference $i_{pri}$ is set to zero and $G_{PRI} = G_{PR} + G_I$ . Here, *i*pri,*k* is the *k*th harmonic in primary current, *i*sec,*k* is the corresponding reflected secondary current. The net *k*th harmonic in the secondary is given by *i*sec,*k* − *i*sec,*k*(0) , which is estimated by the adaptive filter to give *i*sec,*k*,*t* . *i*sec,*k*(0) is the *k*th harmonic current flowing when there was no compensation.

Let *G*(*s*) be the transfer function between *vk*,ref and *i*pri,*k* . This can be expressed from Fig 9 as in (34). Here, *G*plant(*s*) is the plant transfer function as given in (4)

$$G(s) = G\text{plant}(s)$$
$$1 + G\text{plant}(s)G\text{PRI}(s) \quad . \quad (34)$$

$G_{AF}(s)$ is the equivalent transfer function of the adaptive filter tracking *k*th harmonic of the grid current. In order to model $G_{AF}(s)$, consider an adaptive filter which tracks a dc value in a signal. This dc tracking adaptive filter can be modeled as a firstorder transfer function with unity gain and with a time constant *Ta* which depends on the parameter $\mu$. This transfer function is designated as $G_{AF},0\ (s)$ and is given in (35). In order to obtain the transfer function of the adaptive filter tracking *k*th harmonic, low pass to bandpass transformation [36] is used to transform (35). This gives $G_{AF}(s)$ as in (36)

$$G_{AF,0}(s) = \frac{1}{1+sT_a}$$

$$G_{AF}(s) = \frac{2s}{T_a s^2 + 2s + (k\omega_o)^2 T_a}.$$

$$\frac{i_{sec,k,t}}{i^*_{sec,k,t}}(s) = \frac{k_{adapt}G(s)G_{AF}(s)/n}{1 + k_{adapt}G(s)G_{AF}(s)/n}.$$

For the $k_{th}$ harmonic, let the steady value for the transfer function in (37), evaluated at frequency $k_{\omega o}$ have a magnitude $\alpha$,
with $\alpha < 1$. Then

$$\left|\frac{i_{sec,k,t}}{i^*_{sec,k,t}}(jk\omega_o)\right| = \alpha$$

$$\left|\frac{k_{adapt}G(jk\omega_o)G_{AF}(jk\omega_o)/n}{1 + k_{adapt}G(jk\omega_o)G_{AF}(jk\omega_o)/n}\right| = \alpha.$$

$$\text{As } G_{AF}(jk\omega_o) = 1$$

$$k_{adapt} = \frac{\alpha}{1-\alpha}\frac{n}{|G(jk\omega_o)|}.$$

The transfer function $G(jk\omega o)$ for harmonics can be approximated As

$$|G(jk\omega_o)| \approx \frac{1}{|G_{\mathrm{PRI}}(jk\omega_o)|}$$
$$\Rightarrow |G(jk\omega_o)| \approx \frac{1}{K_p}.$$

Using (41) in (40), the final expression for $k$adapt can be obtained as

$$k_{\mathrm{adapt}} = \frac{\alpha}{1-\alpha} n K_p.$$

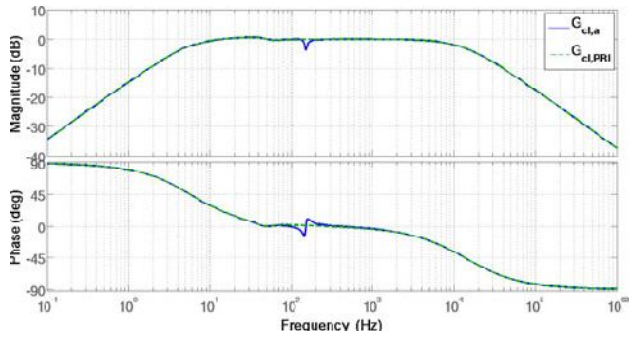


Figure 10. Comparison of an approximate and actual fundamental inverter ac current control transfer function for Ta = 0.03 s, $k_{adapt}$ = 25.6.

For a given value of $\alpha < 1$, it can be shown that, the original $k_{th}$ harmonic in the grid current gets reduced by a factor of $1/(1-\alpha)$. Thus, $k_{adapt}$ can be chosen from (42) depending on the amount of reduction required. The residual distortion after adaptive compensation can be determined as

$$i_{sec},k\ t = i_{sec},k(0) \times (1-\alpha).$$

**B) Interaction between the PRI Controller and the Adaptive Compensation Scheme**

It can be recalled that while designing $K_p$, $K_r$ and $K_i$ , the control block diagram considered in Fig.8 did not include the effect of adaptive compensation. In fact, from Fig. 9, it can be observed that the primary current control is linked to the adaptive compensation section and the actual transfer function for the primary current control including the model for adaptive compensation is

$$G_{cl,a} \triangleq \frac{i_{\mathrm{pri}}}{i^*_{\mathrm{pri}}}$$
$$= \frac{G_{\mathrm{PR}} G_{\mathrm{plant}}}{1 + G_{\mathrm{plant}}(G_{\mathrm{PR}} + G_I + G_{\mathrm{AF}} k_{\mathrm{adapt}}/n)}.$$

To ensure that the fundamental control loop performance is not affected appreciably, the Bode plots of the transfer function $G_{cl}$, $a$ given in (44) and the one used in (14) are compared. Fig.5.10 shows the two Bode plots for the design values as in Table II. As it can be observed, there is no appreciable difference in the two plots.

Note that the extra term appearing in the actual transfer function will modify the overall response near the harmonic frequency range, third harmonic in Fig.5.10. At all other frequency range, the response is practically the same.

As the value of $k_{adapt}$ determines the amount of compensation, the stability of the closed-loop transfer function is analyzed as $k_{adapt}$ varies. This is done by looking at the Routh array of the denominator polynomial in the closed-loop transfer function as given in (44). Now, (44) as a function of $k_{adapt}$ is determined by the transfer function

$$G_{cl,a} = \frac{b_5 s^5 + b_4 s^4 + b_3 s^3 + b_2 s^2 + b_1 s}{a_6 s^6 + a_5 s^5 + a_4 s^4 + a_3 s^3 + a_2 s^2 + a_1 s + a_0}$$

| Coefficient | Value | Coefficient | Value |
|---|---|---|---|
| | | $a_6$ | $151 \times 10^{-6}$ |
| $b_5$ | 12.86 | $a_5$ | 12.9 |
| $b_4$ | 3403 | $a_4$ | $3982 + 19.05k_{adapt}$ |
| $b_3$ | $1.286 \times 10^7$ | $a_3$ | $1.297 \times 10^7$ |
| $b_2$ | $2.346 \times 10^9$ | $a_2$ | $10^6(2782 + 1.880k_{adapt})$ |
| $b_1$ | $1.127 \times 10^{12}$ | $a_1$ | $1.133 \times 10^{12}$ |
| | | $a_0$ | $3.757 \times 10^{13}$ |

Table: II Coefficients in the primary current control transfer function Gc l,a

The coefficients in (45) are provided in Table II. The first column elements of Routh array for the denominator in (45) are

$$\begin{pmatrix} 151.1 \times 10^{-6} \\ 12.9 \\ 3830 + 19.05k_{\mathrm{adapt}} \\ \frac{222.8 \times 10^6 k_{\mathrm{adapt}} + 1.39 \times 10^{10}}{3830 + 19.05k_{\mathrm{adapt}}} \\ \frac{7.8 \times 10^{12} k^2_{\mathrm{adapt}} + 4.9 \times 10^{17} k_{\mathrm{adapt}} + 2.4 \times 10^{19}}{222.8 \times 10^6 k_{\mathrm{adapt}} + 1.39 \times 10^{10}} \\ \frac{7 \times 10^{17} k^2_{\mathrm{adapt}} + 3.6 \times 10^{22} k_{\mathrm{adapt}} + 1.8 \times 10^{24}}{6.2 \times 10^5 k^2_{\mathrm{adapt}} + 3.9 \times 10^{10} k_{\mathrm{adapt}} + 1.9 \times 10^{12}} \\ 3.757 \times 10^{13} \end{pmatrix}$$

As can be observed from (46), there is no sign change in the first column for positive $k_{adapt}$ . This means that the system will be stable for all positive values of $k_{adapt}$ , which is

selected using (42). Thus, the interaction between the PRI loop and the adaptive compensation scheme would not affect the stability of the system, and also as observed from Fig.10 the response for the design values is practically unaffected.

## IV. SIMULATION RESULTS

This section contains the simulation results validating the design procedure proposed in this paper. All the simulation results correspond to one of the four cases of current control that are listed in Table IV

| | |
|---|---|
| Case 1 | No dc offset compensation and no adaptive harmonic compensation |
| Case 2 | No dc offset compensation but adaptive harmonic compensation is implemented |
| Case 3 | DC offset compensation is implemented but no adaptive harmonic compensation |
| Case 4 | Both dc offset compensation and adaptive harmonic compensation are implemented |

Table IV four cases of inverter current control

.

Case 1 has just a PR controller and will have the highest lower order harmonic distortion. Case 2 contains a PR controller and adaptive harmonic compensation. Case 3 contains only a PRI controller but the LMS adaptive filter is disabled. Case 4 contains both the methods proposed in this paper, i.e., the PRI controller and adaptive harmonic compensation using the LMS filter and the proportional controller. This case will have the least lower order harmonic distortion.

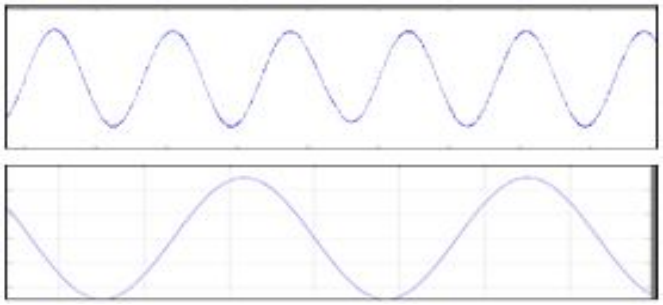

(a)

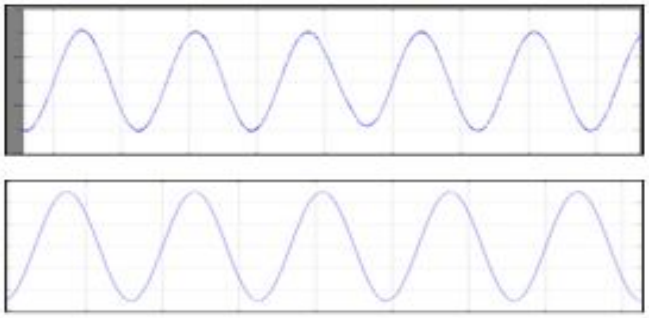

(b)

Figure 11 comparison of grid current (a) case 1: No dc offset compensation and no adaptive harmonic compensation(b) Case 4: Both dc offset compensation and adaptive harmonic compensation are implemented

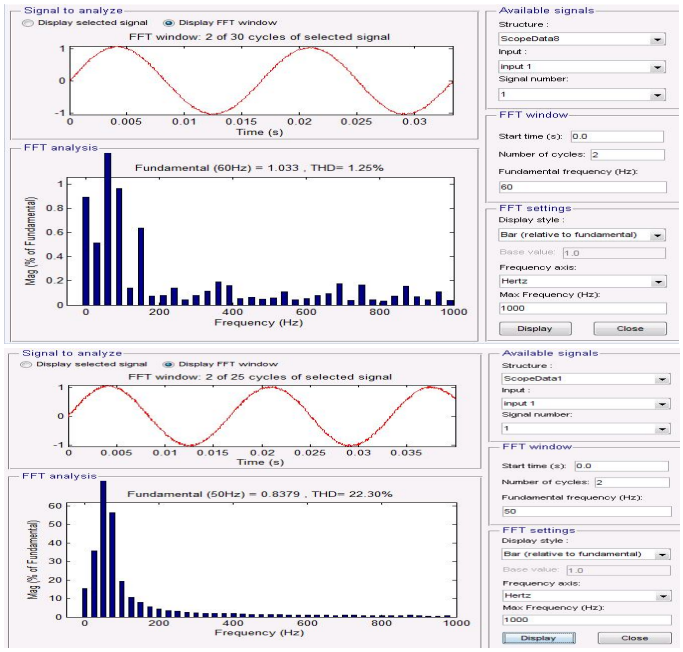


Figure 12 comparison of grid current harmonic spectrum for case 1-No DC offset compensation and No adaptive harmonic compensation case 4-Both DC offset and adaptive harmonic compensation are implemented (when there is no dc offset in control loop)

The distortion is due to the lower order odd harmonics caused predominantly by the distorted transformer magnetizing current. Fig. 11 shows the grid current and sensed grid voltage with voltage sensor gain of 0.01 V/V for the current control method of case 1 as indicated in Table I. The presence of lower order harmonics can be seen from Fig. 11 shows the same set of waveforms when the proposed control scheme is used, which corresponds to case 4 with adaptive compensation applied to third harmonic alone. The improvement in the wave shape can be observed due to the attenuation of the third harmonic.

The harmonic spectrum of the grid current waveform in Fig. 11 is shown in Fig. 12 The reduction in the third harmonic can be observed from the spectrum in Fig.12. The summary of the total harmonic distortion (THD) of the grid current waveform in Fig. 11 is given in Table V.

| Quantity | Without compensation (Case 1) | With compensation (Case2) |
|---|---|---|
| Grid current THD | 8.20% | 4.97% |
| Magnitude of third harmonic | 7.34% | 3.47% |

Table V Comparison of grid current THD and its third harmonic content For cases 1 and 4 when there is no dc offset in the control loop

As mentioned in the TableV , the THD in the grid current has been brought to less than 5% by just using third

harmonic compensation. The third harmonic was reduced from a value of 7.38% to 3.47%. If necessary, by adding adaptive compensation blocks for the higher harmonics, the THD of grid current can be further improved.

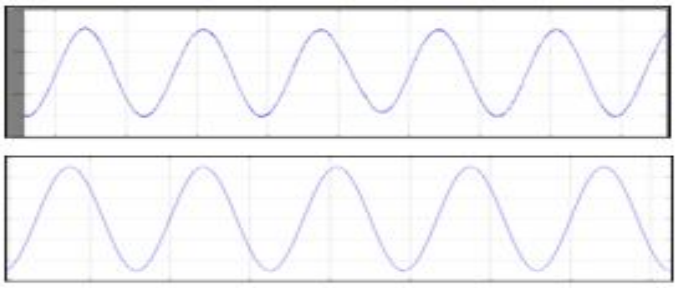

(a)

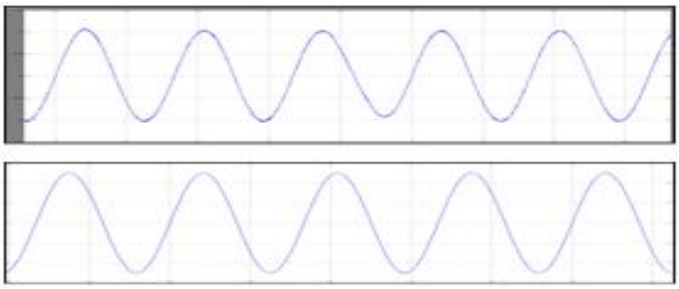

(b)

Figure 13 comparison of grid current (a) case 1-No DC offset compensation and No adaptive harmonic compensation case 4-Both DC offset compensation and adaptive harmonic compensation are implemented

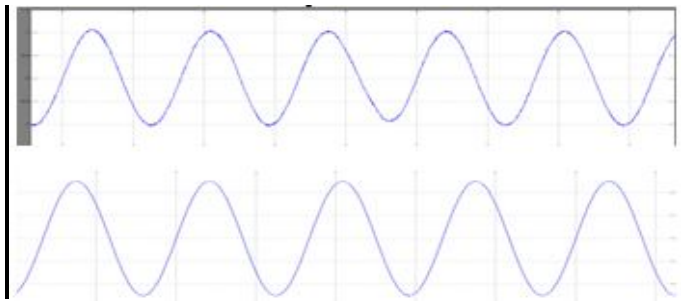

(a)

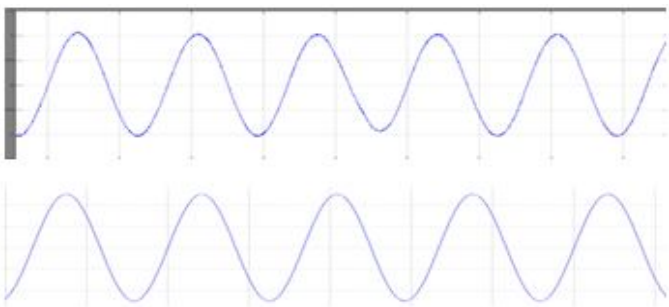

(b)

Figure 14 comparison of grid current when there is a DC offset in control loop (a)case 1-No DC offset and No adaptive harmonic compensation (b) case 4-Both DC offset and adaptive harmonic compensation are implemented

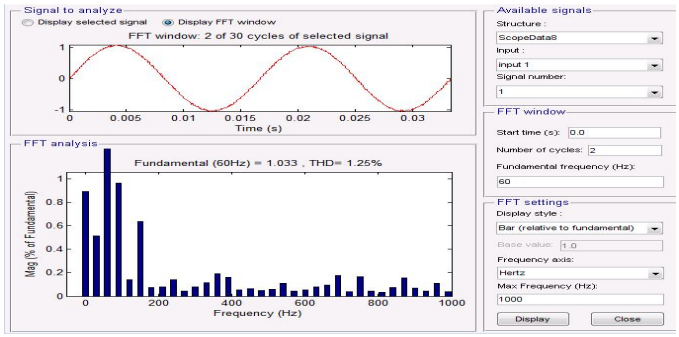


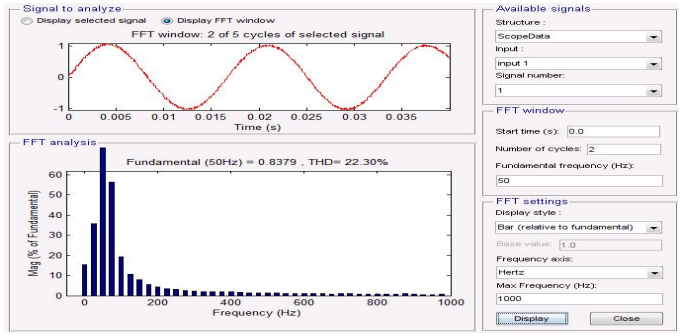


Figure 15 comparison of grid current harmonic spectrum when there is a dc offset in control loop For case 1-No DC offset compensation and No adaptive harmonic compensation case 4-Both DC offset and adaptive harmonic compensation are implemented

For the same situation, Fig.13 shows the primary current and the sensed grid voltage. Primary current for case 1 is of a better quality, as can be seen from Fig. 13(a). This is because the dominant cause for distortion in this system is the distorted transformer magnetizing current. This was drawn from the grid in case 1. From Fig. 13(b), it is clear that the harmonics are added to the primary current and it is more distorted. In other words, the distortion has been transferred from the grid current to the primary-side current, which improves the grid current as seen in Fig. 11(b).

The control loop was not having any offset for the results shown in Figs. 11 and 12. In other words, the performance would have been the same even when the PR controller was used in place of the proposed PRI controller. To show the effectiveness of the PRI controller, an offset was added to the control loop. As explained in Section II, this offset will introduce even harmonic in the grid current. Thus, the next set of waveforms shown in Figs. 14 and 15 is for the case when the control loop contains a dc offset. Here, the distortion in the uncompensated case, i.e., case 1 is very pronounced due to the presence of significant even harmonics in addition to the odd harmonics as can be seen in Fig. 15(a). Fig. 14(b) shows the grid current for the same situation but with full compensation, i.e., case 4. It can be clearly seen that Fig. 14(a) has even harmonics whereas in Fig. 14(b) the even

harmonics are practically negligible. This is confirmed in the spectrum of grid current shown in Fig. 15. In the dc in primary current is compared when the primary current control loop has a dc offset. As it can be observed, the PRI controller practically eliminates the dc component.

## V. CONCLUSION

Modification to the inverter current control for a grid connected single-phase photovoltaic inverter has been proposed in this paper, for ensuring high quality of the current injected into the grid. For the power circuit topology considered, the dominant causes for lower order harmonic injection are identified as the distorted transformer magnetizing current and the dead time of the inverter. It is also shown that the presence of dc offset in control loop results in even harmonics in the injected current for this topology due to the dc biasing of the transformer.

A novel solution is proposed to attenuate all the dominant lower order harmonics in the system. The proposed method uses an LMS adaptive filter to estimate a particular harmonic in the grid current that needs to be attenuated. The estimated current is converted into an equivalent voltage reference using a proportional controller and added to the inverter voltage reference. The design of the gain of a proportional controller to have an adequate harmonic compensation has been explained. To avoid dc biasing of the transformer, a novel PRI controller has been proposed and its design has been presented.

The interaction between the PRI controller and the adaptive compensation scheme has been studied. It is shown that there is minimal interaction between the fundamental current controller and the methods responsible for dc offset compensation and adaptive harmonic compensation. The PRI controller and the adaptive compensation scheme together improve the quality of the current injected into the grid.

The complete current control scheme consisting of the adaptive harmonic compensation and the PRI controller has been verified experimentally and the results show good improvement in the grid current THD once the proposed current control is applied. The transient response of the whole system is studied by considering the startup transient and the overall performance is found to agree with the theoretical analysis. It may be noted here that these methods can be used for other applications that use a line interconnection transformer wherein the lower order harmonics have considerable magnitude and need to be attenuated.

## REFERENCES

[1] Mitigation of lower order Harmonics in a grid connected single phase PV inverter “IEEE transactions on power electronics vol.28,no 11,november 2013”

[2] S. B. Kjaer, J. K. Pedersen, and F. Blaabjerg, “A review of single-phase grid-connected inverters for photovoltaic modules,” IEEE Trans. Ind. Appl., vol. 41, no. 5, pp. 1292–1306, Sep./Oct. 2005.

[3] S.-G. Jeung and M.-H. Park, “The analysis and compensation of deadtime effects in PWM inverters,” IEEE Trans. Ind. Electron., vol. 38, no. 2, pp. 108–114, Apr. 1991.

[4] J.-W. Choi and S.-K. Sul, “A new compensation strategy reducing voltage current distortion in PWM VSI systems operating with low output voltages,” IEEE Trans. Ind. Appl., vol. 31, no. 5, pp. 1001–1008, Sep./Oct. 1995.

[5] A. R.Mu˜noz and T. A. Lipo, “On-line dead-time compensation technique for open-loop PWM-VSI drives,” IEEE Trans. Power Electron., vol. 14, no. 4, pp. 683–689, Jul. 1999.

[6] A. C. Oliveira, C. B. Jacobina, and A. M. N. Lima, “Improved dead-time compensation for sinusoidal PWM inverters operating at high switching frequencies,” IEEE Trans. Ind. Electron., vol. 54, no. 4, pp. 2295–2304, Aug. 2007.

[7] L. Chen and F. Z. Peng, “Dead-time elimination for voltage source inverters,” IEEE Trans. Power Electron., vol. 23, no. 2, pp. 574–580, Mar. 2008.

[8] IEEE Recommended Practices and Requirements for Harmonic Control in Electrical Power Systems, IEEE Standard 519-1992, 1992.

[9] IEEE Standard for Interconnecting Distributed Resources With the Electric Power System, IEEE Standard 1547-2003, 2003.

[10] T. Esram and P. L. Chapman, “Comparison of photovoltaic array maximum power point tracking techniques,” IEEE Trans. Energy Convers., vol. 22, no. 2, pp. 439–449, Jun. 2007.

[11] R. Kadri, J.-P. Gaubert, and G. Champenois, “An improved maximum power point tracking for photovoltaic grid-connected inverter based on voltage-

oriented control," IEEE Trans. Ind. Electron., vol. 58, no. 1, pp. 66–75, Jan. 2011.

[12] T. Kitano, M. Matsui, and D. Xu, "Power sensorlessMPPT control scheme utilizing power balance at DC link—System design to ensure stability and response," in Proc. 27th Annu. Conf. IEEE Ind. Electron. Soc., 2001, vol. 2, pp. 1309–1314.

[13] Y. Chen and K. M. Smedley, "A cost-effective single-stage inverter with maximum power point tracking," IEEE Trans. Power Electron., vol. 19, no. 5, pp. 1289–1294, Jun. 2004.

[14] Q. Mei, M. Shan, L. Liu, and J. M. Guerrero, "A novel improved variable step-size incremental-resistance MPPT method for PV systems," IEEE Trans. Ind. Electron., vol. 58, no. 6, pp. 2427–2434, Jun. 2011.

[15] A. K. Abdelsalam, A. M. Massoud, S. Ahmed, and P. N. Enjeti, "High-performance adaptive perturb and observe MPPT technique for photovoltaic-based microgrids," IEEE Trans. Power Electron., vol. 26, no. 4, pp. 1010–1021, Apr. 2011.

[16] P. Mattavelli, "A closed-loop selective harmonic compensation for active filters," IEEE Trans. Ind. Appl., vol. 37, no. 1, pp. 81–89, Jan./Feb. 2001.

[17] X. Yuan, W. Merk, H. Stemmler, and J. Allmeling, "Stationary-frame generalized integrators for current control of active power filters with zero steady-state error for current harmonics of concern under unbalanced and distorted operating conditions," IEEE Trans. Ind. Appl., vol. 38, no. 2, pp. 523–532, Mar./Apr. 2002.

[18] J. Allmeling, "A control structure for fast harmonics compensation in active filters," IEEE Trans. Power Electron., vol. 19, no. 2, pp. 508–514, Mar. 2004.

[19] C. Lascu, L. Asiminoaei, I. Boldea, and F. Blaabjerg, "High performance current controller for selective harmonic compensation in active power filters," IEEE Trans. Power Electron., vol. 22, no. 5, pp. 1826–1835, Sep. 2007.

[20] D. De and V. Ramanarayanan, "A proportional + multiresonant controller for three-phase four-wire high-frequency link inverter," IEEE Trans. Power Electron., vol. 25, no. 4, pp. 899–906, Apr. 2010.

[21] R. C´ardenas, C. Juri, R. Pen˜na, P.Wheeler, and J. Clare, "The application of resonant controllers to four-leg matrix converters feeding unbalanced or nonlinear loads," IEEE Trans. Power Electron., vol. 27, no. 3, pp. 1120– 1128, Mar. 2012.

[22] A. G. Yepes, F. D. Freijedo, O´ . Lo´pez, and J. Doval-Gandoy, "Highperformance digital resonant controllers implemented with two integrators," IEEE Trans. Power Electron., vol. 26, no. 2, pp. 563–576, Feb. 2011.

[23] A. G. Yepes, F. D. Freijedo, J. Doval-Gandoy, O. Lopez, J. Malvar, and P. Fernandez-Comesa˜na, "Effects of discretization methods on the performance of resonant controllers," IEEE Trans. Power Electron., vol. 25, no. 7, pp. 1692–1712, Jul. 2010.

[24] P. Mattavelli and F. P.Marafao, "Repetitive-based control for selective harmonic compensation in active power filters," IEEE Trans. Ind. Electron., vol. 51, no. 5, pp. 1018–1024, Oct. 2004.

[25] R. Costa-Costello, R. Grino, and E. Fossas, "Odd-harmonic digital repetitive control of a single-phase current active filter," IEEE Trans. Power Electron., vol. 19, no. 4, pp. 1060–1068, Jul. 2004.

[26] S. Jiang, D. Cao, Y. Li, J. Liu, and F. Z. Peng, "Low-THD, fast-transient, and cost-effective synchronous-frame repetitive controller for three-phase UPS inverters," IEEE Trans. Power Electron., vol. 27, no. 6, pp. 2994– 3005, Jun. 2012.

[27] J. M. Olm, G. A. Ramos, and R. Costa-Costel´o, "Stability analysis of digital repetitive control systems under time-varying sampling period," IET Control Theor. Appl., vol. 5, no. 1, pp. 29–37, Jan. 2011.

[28] M. Cirrincione, M. Pucci, G. Vitale, and A. Miraoui, "Current harmonic compensation by a single-phase shunt active power filter controlled by adaptive neural filtering," IEEE Trans. Ind. Electron., vol. 56, no. 8, pp. 3128–3143, Aug. 2009.

[29] B. Singh and J. Solanki, "An implementation of an adaptive control algorithm for a three-phase shunt active filter," IEEE Trans. Ind. Electron., vol. 56, no. 8, pp. 2811–2820, Aug. 2009.

[30] L. Qian, D. A. Cartes, and H. Li, "An improved adaptive detectionmethod for power quality improvement," IEEE Trans. Ind. Appl., vol. 44, no. 2, pp. 525–533, Mar./Apr. 2008.

[31] S.-Y. Kim and S.-Y. Park, "Compensation of dead-time effects based on adaptive harmonic filtering in the vector-controlled AC motor drives," IEEE Trans. Ind. Electron., vol. 54, no. 3, pp. 1768–1777, Jun. 2007.

[32] V. Blasko, "A novel method for selective harmonic elimination in power electronic equipment," IEEE Trans. Power Electron., vol. 22, no. 1, pp. 223–228, Jan. 2007.

[33] A. E. Fitzgerald, C. Kingsley Jr, and S. D. Umans, Electric Machinery, 6th ed. New York: McGraw-Hill, 2003.

[34] J. D. Aspnes, R. P. Merritt, and S. I. Akasofu, "Harmonic generation in transformers related to DC excitation and system loading," IEEE Trans. Power Appl. Syst., vol. PAS-100, no. 4, pp. 1845–1851, Apr. 1981.

[35] S. Lu, Y. Liu, and J. De La Ree, "Harmonics generated from a DC biased transformer," IEEE Trans. Power Del., vol. 8, no. 2, pp. 725–731, Apr. 1993.

[36] J. A. Orr and A. E. Emanuel, "On the need for strict second harmonic limits," IEEE Trans. Power Del., vol. 15, no. 3, pp. 967–971, Jul. 2000.

[37] D. N. Zmood and D. G. Holmes, "Stationary frame current regulation of PWMinverterswith zero steady-state error," IEEE Trans. Power Electron., vol. 18, no. 3, pp. 814–822, May 2003.

[38] J. R. Glover Jr., "Adaptive noise cancelling applied to sinusoidal interferences," IEEE Trans. Acoust., Speech, Signal Process., vol. 25, no. 6, pp. 484–491, Dec. 1977.

[39] M. Ciobotaru, R. Teodorescu, and F. Blaabjerg, "A new single phase PLL structure based on second order generalized integrator," in Proc. 37th IEEE Power Electron. Spec. Conf., Jun. 2006, pp. 1–6.